Research Article

Maya Briani, Christopher Anthony Denaro, Benedetto Piccoli, and Luigi Rarità*

Dynamics of particulate emissions in the presence of autonomous vehicles

https://doi.org/10.1515/math-2024-0126
received November 21, 2024; accepted December 31, 2024

Abstract: Around one third of CO_2 emissions in the atmosphere are linked to vehicular traffic. Pollutant agents have an impact on the environment, in particular, the increased presence of particulate matter (PM) creates negative effects on human health. This article examines how autonomy could positively reduce the emission of air pollutants due to traffic. The methodology involves the analyses of PM emissions as a function of traffic conditions, especially in the presence of autonomous vehicles (AVs) dampening traffic waves. The starting point is traffic measurements that, gathered from real experiments involving a fleet of vehicles moving on a ring track, exhibit the presence of stop-and-go waves that are dampened by control strategies implemented on a unique AV. Using a system of ordinary differential equations modeling the principal chemical reactions in the atmosphere, it is proved that wave dampening implies a significant decrease in PM emissions at ground level. The horizontal diffusion of the pollutants is estimated by partial differential equations combined with the model for chemical reactions. The obtained outcomes show advantages given by the improvements in traffic flows and the mitigation effect of green barriers.

Keywords: road traffic, emissions, particulate matter, ordinary and partial differential equations

MSC 2020: 34A34, 35K57, 62P12

1 Introduction

Within the context of road traffic, emissions provide high contributions to particulate matter (PM) concentrations in urban areas. It is known that exposures to PM due to vehicular emissions have negative effects on the environment [1–3], especially on human health. PM from road traffic includes exhaust emissions, namely contributions from the tailpipe, and non-exhaust emissions due to wear and tear of some vehicle parts, such as suspension of dust, tires, brake, and clutch. PM is of various types according to the aerodynamic diameter. For instance, $PM_{2.5}$ and PM_{10} have, respectively, particles with diameters less than or equal to 2.5 and 10 μm. Thus, PM_{10} consists of particles between 2.5 and 10 μm and less than 2.5 μm, hence clear distinctions for possible classifications are not fully possible. From experimental studies, $PM_{2.5}$ is the result of combustion of fossil fuels, such as motor vehicle exhaust [4,5], while PM_{10} is mainly due to deserts, natural sources (i.e., fires for instance), and human actions, such as industrial emissions and road dust [6,7]. While coarse particles are easy to remove from the atmosphere via dry and wet deposition, the situation is the opposite for fine particles that are inhaled

* **Corresponding author: Luigi Rarità,** Dipartimento di Scienze Aziendali-Management and Information Systems, University of Salerno, Via Giovanni Paolo II, 132, Fisciano (SA), 84084, Italy, e-mail: lrarita@unisa.it
Maya Briani: Consiglio Nazionale delle Ricerche, Istituto per le Applicazioni del Calcolo Mauro Picone, Via dei Taurini, 19, Rome, 00185, Italy, e-mail: m.briani@iac.cnr.it
Christopher Anthony Denaro: Center for Computational and Integrative Biology, Rutgers University-Camden, 201 S. Broadway, Camden, 08102, New Jersey, USA, e-mail: cad373@scarletmail.rutgers.edu
Benedetto Piccoli: Department of Mathematical Sciences, Rutgers University-Camden, 311 N. Fifth Street, Camden, 08102, New Jersey, USA, e-mail: piccoli@camden.rutgers.edu

by humans [8,9]. Within this framework, possible techniques for the estimation of PM concentrations in the atmosphere become important for either control strategies of air pollution or life quality. Such issues represent a hard task for the complex dynamics in the atmosphere and most of the research topics focus on exhaust emissions [10,11], while non-exhaust PM emissions are still under investigation [12].

In this article, the PM emissions are analyzed in some experimental cases that are similar to those described in [13,14]. The intention [15] is to understand how driving activities create meaningful impacts on common traffic phenomena, such as the formation of traffic jams, fuel consumption (FC), and pollution. Precisely, a special focus is addressed to the presence of autonomous vehicles (AVs), [16], and their influence on emissions [17]. In this framework, various aspects are often considered: control techniques for optimal routing and traffic flows [18], efficiency for combustion engine [19], adoption of hybrid vehicles in road networks [20], climate changes as a result of emissions [21], stop-and-go waves [22], and possible traffic instabilities. As for estimations of pollutants starting from emissions [23,24], a valid solution is provided by either aggregate or microscopic models dealing with instantaneous measurements for vehicles [25–27].

The contribution of this article is as follows. Focusing on data measurements from traffic experiments, reported in [28,29], a general microscopic model [30] is used to prove that a single AV inside a fleet allows a decrease of PM emissions. Then, a system of ordinary differential equations (ODEs) is defined from the chemical reactions involving PM in the atmosphere [31,32]. The system is solved numerically and the concentrations of pollutants at ground level confirm the emission reductions. FC reduces as well. Then, partial differential equations (PDEs) are considered to model the horizontal diffusion of the various pollutant agents [33]. In this case, variations in a reference domain are studied in the presence of wind and green walls that should act as sinks and barriers for pollutants. We obtain expected and unexpected features. On one hand, barriers provide a protective effect against the diffusion. On the other hand, the protection effect depends on the specific chemical species. In particular, for ozone and PM, we have two different phenomena: the former is highly shielded, while only partial protection occurs for the latter. Indeed, PM spreads from the roads in higher percentages, thus risking negative effects on human health.

The coupling of a classical emission model with the dynamics of chemical species in terms of ODEs/PDEs represents the main novelty of the presented work. The outcome is an approach that models traffic phenomena and variations of pollutants in the atmosphere, with emphasis on diffusion effects in urban regions.

We conclude that control strategies run on AVs inside a fleet allow a significant decrease of particulate at ground level. For horizontal diffusion, green barriers represent a good strategy to shield harmful effects deriving from only some types of pollutants. For PM, which is the result of multiple atmospheric and human actions, the screening effect is limited and further future analyses are needed.

The article is structured as follows. Section 2 describes a possible model for PM emissions and concentrations of pollutants either at ground level or horizontally. Section 3 shows the features of the experiments used as case studies. Section 4 contains numerical results about PM emissions and the evolution of pollutants. Conclusions and future research activities end the article in Section 5.

2 Models for emissions and concentrations of pollutants

This section presents some approaches to model PM emissions and concentration of principal pollutants. The corresponding chemical reactions, harmful for humans [34,35], often occur in sunlight environments [36,37] and involve either nitrogen oxide (NO_x), that in turn generate ozone, or sulfur oxide (SO_x) emissions.

First, PM emissions are analyzed. Then, ODEs and PDEs are proposed for the evolution of pollutants at ground level and in the air.

2.1 A model for particulate emissions

Focus on the microscopic emission model described in [30]. Given a generic petrol vehicle j with instantaneous speed $v_j(t)$ [m/s] and acceleration $a_j(t)$ [m/s^2], the corresponding PM emissions are estimated as:

$$E_j^{\mathrm{PM}}(t) = \max\{\psi_1 v_j(t) + \psi_2 v_j^2(t) + \psi_3 a_j^2(t) + \psi_4 v_j(t) a_j(t), \psi_5\},$$

where ψ_i, $i = 1,\dots,4$, are as follows for an internal combustion engine:

$$\psi_1 = 1.57\cdot 10^{-5}\ \mathrm{g/m}, \qquad \psi_2 = -9.21\cdot 10^{-7}\ \mathrm{g\ s/m^2},$$
$$\psi_3 = 3.75\cdot 10^{-5}\ \mathrm{g\ s^3/m^2}, \quad \psi_4 = 1.89\cdot 10^{-5}\ \mathrm{g\ s^2/m^2},$$

while ψ_5 represents an emission lower-bound, assumed zero in case of using ψ_i, $i = 1,\dots,4$. The overall PM emission for a fleet of N vehicles is as follows:

$$E^{\mathrm{PM}}(t) = \sum_{i=1}^{N} E_j^{\mathrm{PM}}(t). \tag{1}$$

Note that (1) is a combination of polynomials in velocities and accelerations. This allows possible extensions and adaptations to other different emission models (see [38] for further details).

2.2 Production of pollutants

Chemical reactions for particulate deal with different gases, including NO_x and SO_x. The formation of nitrogen oxides involves atomic oxygen (O), oxygen (O_2), and nitrogen (N_2) with consequent production of ozone O_3. We focus on the following reactions for the ground-level ozone formation due to nitrogen oxides:

$$\mathrm{NO_2} \xrightarrow{k_1} \mathrm{O + NO}, \tag{2}$$

$$\mathrm{O + 2O_2} \xrightarrow{k_2} \mathrm{O_3 + O_2}, \tag{3}$$

$$\mathrm{NO + O_3} \xrightarrow{k_3} \mathrm{NO_2 + O_2}, \tag{4}$$

where, indicating by mol the number of molecules, k_1, k_2, and k_3 are the following kinetic constants [39]:

$$k_1 = 0.02\ \mathrm{s^{-1}},$$
$$k_2 = 6.09\cdot 10^{-34}\,\mathrm{cm^6\ mol^{-2}\ s^{-1}},$$
$$k_3 = 1.81\cdot 10^{-14}\,\mathrm{cm^3\ mol^{-1}\ s^{-1}}.$$

From reaction (2), NO_2 is photo-dissociated into O. The creation of O_3 is due to (3). Finally, from (4), O_3 is transformed into NO_2 and O_2. Further remarks about the principal chemical processes for the cycles of O_3 due to NO_x are fully described in [32] and [33].

For the deterioration of NO_x and the evolution of SO_x in the atmosphere, we also consider the following reactions [40,41]:

$$\mathrm{NO_2 + O} \xrightarrow{k_n} \mathrm{NO + O_2}, \tag{5}$$

$$\mathrm{SO + O_2} \xrightarrow{k_{s_1}} \mathrm{SO_2 + O}, \tag{6}$$

$$\mathrm{SO_2 + O_3} \xrightarrow{k_{s_2}} \mathrm{SO_3 + O_2}, \tag{7}$$

with [39]:

$$k_n = 9.72\cdot 10^{-12}\,\mathrm{cm^3\ mol^{-1}\ s^{-1}}, \quad k_{s_1} = 2.1\cdot 10^{-12}\,\mathrm{cm^3\ mol^{-1}\ s^{-1}}, \quad k_{s_2} = 1.5\cdot 10^{-19}\,\mathrm{cm^3\ mol^{-1}\ s^{-1}}.$$

Note that, while (6) and (7) describe the whole cycle for the dynamics of sulfur oxides, equation (5) indicates the decay of nitrogen dioxide, hence completing the atmospheric process involving NO_x and ozone. Representing by $[\cdot]$ the concentration (in terms of weight unit/volume unit) vs time of a generic chemical species, we have the following ODEs from reactions (2), (3), and (4):

$$\frac{\mathrm{d}}{\mathrm{d}t}[\mathrm{O}] = k_1[\mathrm{NO_2}] - k_2[\mathrm{O}][\mathrm{O_2}]^2, \tag{8}$$

$$\frac{\mathrm{d}}{\mathrm{d}t}[\mathrm{O_2}] = -k_2[\mathrm{O}][\mathrm{O_2}]^2 + k_3[\mathrm{O_3}][\mathrm{NO}], \tag{9}$$

$$\frac{\mathrm{d}}{\mathrm{d}t}[\mathrm{O_3}] = k_2[\mathrm{O}][\mathrm{O_2}]^2 - k_3[\mathrm{O_3}][\mathrm{NO}], \tag{10}$$

$$\frac{\mathrm{d}}{\mathrm{d}t}[\mathrm{NO}] = k_1[\mathrm{NO_2}] - k_3[\mathrm{O_3}][\mathrm{NO}], \tag{11}$$

$$\frac{\mathrm{d}}{\mathrm{d}t}[\mathrm{NO_2}] = -k_1[\mathrm{NO_2}] + k_3[\mathrm{O_3}][\mathrm{NO}]. \tag{12}$$

From (5), (6), and (7), we obtain

$$\frac{\mathrm{d}}{\mathrm{d}t}[\mathrm{O}] = k_{s_1}[\mathrm{SO}][\mathrm{O_2}] - k_n[\mathrm{NO_2}][\mathrm{O}], \tag{13}$$

$$\frac{\mathrm{d}}{\mathrm{d}t}[\mathrm{O_2}] = -k_{s_1}[\mathrm{SO}][\mathrm{O_2}] + k_n[\mathrm{NO_2}][\mathrm{O}] + k_{s_2}[\mathrm{SO_2}][\mathrm{O_3}], \tag{14}$$

$$\frac{\mathrm{d}}{\mathrm{d}t}[\mathrm{O_3}] = -k_{s_2}[\mathrm{SO_2}][\mathrm{O_3}], \tag{15}$$

$$\frac{\mathrm{d}}{\mathrm{d}t}[\mathrm{NO}] = k_n[\mathrm{NO_2}][\mathrm{O}], \tag{16}$$

$$\frac{\mathrm{d}}{\mathrm{d}t}[\mathrm{NO_2}] = -k_n[\mathrm{NO_2}][\mathrm{O}] - k_n[\mathrm{NO_2}], \tag{17}$$

$$\frac{\mathrm{d}}{\mathrm{d}t}[\mathrm{SO}] = -k_{s_1}[\mathrm{SO}][\mathrm{O_2}], \tag{18}$$

$$\frac{\mathrm{d}}{\mathrm{d}t}[\mathrm{SO_2}] = k_{s_1}[\mathrm{SO}][\mathrm{O_2}] - k_{s_2}[\mathrm{SO_2}][\mathrm{O_3}] - k_{s_2}[\mathrm{SO_2}], \tag{19}$$

$$\frac{\mathrm{d}}{\mathrm{d}t}[\mathrm{SO_3}] = k_{s_2}[\mathrm{SO_2}][\mathrm{O_3}]. \tag{20}$$

Equations (13)–(20) show that concentrations of O, O_2, O_3, NO_x, and SO_x evolve following the dynamics of $[SO][O_2]$, $[SO_2][O_3]$, and $[NO_2][O]$. In equations (17) and (19), we also consider the damping terms, $k_n[NO_2]$ and $k_{s_2}[SO_2]$, respectively, to model the decay phenomena of the principal pollutant agents. These additive terms are necessary to avoid unbounded growth and reflect the natural decay of molecules. As sulfur oxides depend on O, O_2, and O_3, that also appear in reactions for nitrogen oxides, equations (13)–(20) provide a unique model for the contemporary evolution of NO_x and SO_x and, hence, for PM_{10} and $PM_{2.5}$. With this aim, assuming that all reactions occur in a volume of dimension Δx^3, we define the source term $S^P(t)$ for the pollutant $P \in \{NO_x, SO_x, PM\}$ as follows:

$$S^P(t) \coloneqq \frac{E^P(t)}{\Delta x^3}, \tag{21}$$

where $E^P(t)$ coincides with (1) in case of particulate, while the corresponding expressions for nitrogen and sulfur oxides are discussed in [30].

The particulate has primary components due to $S^{\mathrm{PM}}(t)$ and secondary contributions mainly depending on NO_x and SO_x in the atmosphere. Concentrations of nitrogen and sulfur oxides are not always precisely predictable for PM_{10}, see [8], hence we impose that:

$$\frac{\mathrm{d}}{\mathrm{d}t}[\mathrm{PM}_{10}] = \alpha_1[\mathrm{NO}_2] + \alpha_2[\mathrm{SO}_2] - k_n[\mathrm{PM}_{10}] + S^{\mathrm{PM}}(t), \tag{22}$$

where the coefficients $0 < \alpha_i < 1$, $i = 1, 2$, $\alpha_1 + \alpha_2 = 1$, modulate the contributions of NO_2 and SO_2, and the term $k_n[PM_{10}]$ describes the damping phenomena which model the natural decay of the pollutant over time. For $PM_{2.5}$, we have that [42]:

$$\frac{\mathrm{d}}{\mathrm{d}t}[\mathrm{PM}_{2.5}] = \beta\frac{\mathrm{d}}{\mathrm{d}t}[\mathrm{PM}_{10}], \tag{23}$$

where $\beta = 0.62$. Coupling ODEs (8)–(12) for the cycles of O_3 due to NO_x to equations (13)–(20), we obtain the following final system for the concentrations of pollutants at ground level:

$$\begin{aligned}
[\mathrm{O}]' &= k_2[\mathrm{O}][\mathrm{O}_2]^2 + k_1[\mathrm{NO}_2] + k_{s_1}[\mathrm{O}_2][\mathrm{SO}] - k_n[\mathrm{NO}_2][\mathrm{O}],\\
[\mathrm{O}_2]' &= k_2[\mathrm{O}][\mathrm{O}_2]^2 + k_3[\mathrm{O}_3][\mathrm{NO}] - k_{s_1}[\mathrm{O}_2][\mathrm{SO}] + k_n[\mathrm{NO}_2][\mathrm{O}] + k_{s_2}[\mathrm{SO}_2][\mathrm{O}_3],\\
[\mathrm{O}_3]' &= k_2[\mathrm{O}][\mathrm{O}_2]^2 - k_3[\mathrm{O}_3][\mathrm{NO}] - k_{s_2}[\mathrm{SO}_2][\mathrm{O}_3],\\
[\mathrm{NO}]' &= k_1[\mathrm{NO}_2] - k_3[\mathrm{O}_3][\mathrm{NO}] + k_n[\mathrm{NO}_2][\mathrm{O}] + (1-p)S^{\mathrm{NO}_x}(t),\\
[\mathrm{NO}_2]' &= k_1[\mathrm{NO}_2] + k_3[\mathrm{O}_3][\mathrm{NO}] - k_n[\mathrm{NO}_2][\mathrm{O}] - k_n[\mathrm{NO}_2] + pS^{\mathrm{NO}_x}(t),\\
[\mathrm{SO}]' &= k_s[\mathrm{O}_2][\mathrm{SO}] + q_1S^{\mathrm{SO}_x}(t),\\
[\mathrm{SO}_2]' &= k_s[\mathrm{O}_2][\mathrm{SO}] - k_{s_2}[\mathrm{SO}_2][\mathrm{O}_3] - k_{s_2}[\mathrm{SO}_2] + q_2S^{\mathrm{SO}_x}(t),\\
[\mathrm{SO}_3]' &= k_{s_2}[\mathrm{SO}_2][\mathrm{O}_3] + q_3S^{\mathrm{SO}_x}(t),\\
[\mathrm{PM}_{10}]' &= \alpha_1[\mathrm{NO}_2] + \alpha_2[\mathrm{SO}_2] - k_n[\mathrm{PM}_{10}] + S^{\mathrm{PM}}(t),\\
[\mathrm{PM}_{2.5}]' &= \beta[\mathrm{PM}_{10}]',
\end{aligned} \tag{24}$$

where $p = 0.15$ (see [43]) indicates the percentages of NO_2, and $q_i \in [0, 1]$, $q_1 + q_2 + q_3$ modulate the contributions of SO_x.

Note that system (24) can be rewritten as:

$$\boldsymbol{\Gamma}'(t) = \mathbf{G}(\boldsymbol{\Gamma}(t)) + \mathbf{s}(t),$$

where $\boldsymbol{\Gamma}$ and $\mathbf{s}$ are the vectors that contain, respectively, the concentrations of pollutants and the source terms, the latter being of the type (21), while $\mathbf{G}$ is the matrix that describes the reactions.

2.3 Horizontal diffusion

To model the horizontal diffusion of pollutants, we focus on a horizontal domain $\Omega = [0, L_x] \times [0, L_y]$, where L_x and L_y are, respectively, the length of the road and of the area transversal to the road where, in $[0, T]$, the pollutant agents spread. Assume that $\boldsymbol{\Gamma}$, $\mathbf{G}$, and $\mathbf{s}$ represent the same quantities described in the previous paragraph, and that $\boldsymbol{\Gamma}$ is constant along the third direction so that the model becomes two-dimensional. We obtain the following reaction-diffusion problem for the horizontal diffusion of pollutants:

$$\boldsymbol{\Gamma}' + \mathbf{w}\nabla\boldsymbol{\Gamma} - \mu\Delta\boldsymbol{\Gamma} = \mathbf{G}(\boldsymbol{\Gamma}) + \mathbf{s}, \tag{25}$$

where μ is the diffusion coefficient, assumed the same for all chemical species and equal to 10^{-8} km^2/h for aerosols, see [44]; $\mathbf{w} = (w_x, w_y)$ is a vector that models the wind direction. We consider assigned initial data, while the boundary of Ω considers homogeneous boundary Neumann conditions for all chemical species in consideration. For a suitable treatment of the source term $\mathbf{s}$, that involves contributions for NO_x, SO_x and particulate, see details in [33].

For our analysis, we integrate equation (25) over a uniformly discretized, rectangular domain with holes, that correspond to "green barriers," to estimate the entity of diffusion of the various pollutant agents. Note that

we may consider other types of vegetations besides green barriers. For instance, high-level green infrastructures (such as trees) represent an interesting case study to mitigate the spread of pollutants. However, in [45], it is shown that trees may harm air quality, especially in street canyon environments. Hence, further investigations are needed.

3 Case studies

This section briefly describes the traffic experiments used for the analyses of emissions and concentration of pollutants obtained from the estimations of trajectories of the involved vehicles.

We consider different cases dealing with a fleet of 21 or 22 vehicles that circulate on a ring road in a parking lot in Tucson (Arizona). The fleet has a unique AV that is a Ford Escape Hybrid, while make and model of other cars are as follows: Chevrolet Malibu, Chevrolet Malibu Limited, Chevrolet Impala, Chevrolet Silverado, Chevrolet Suburban, and Dodge Grand Caravan. All trajectories of vehicles are first recorded by a video recording system at the center of the ring track and then estimated via a suitable computer vision algorithm [15].

The basic steps of the experiments are summarized as follows. Setup: All vehicles are uniformly distributed along the ring track; pilots are asked to turn the data recorders in their vehicles; further additive instructions are provided to the various drivers through the windows. Evacuation: the camera at the center of the track is activated and all research group personnel leave the track. Initialize: A horn warns all drivers to change gears from Park to Drive, remaining stopped. Drive: A horn sounds to instruct all pilots to start driving. Stop: An air horn sounds to indicate drivers a safe stop and change gears into Park. Conclusion: the research group personnel enter the track; each pilot stops his vehicle and turns off the in-board recorder; the central camera is deactivated.

Note that, during each experiment, the pilot of the AV is asked to activate a control strategy (autonomous driving or driving velocity change) in the presence of stop-and-go waves; after a certain time from the beginning of the experiment, the control of the AV is disabled and dampening phenomena are evaluated.

Figure 1 shows some photographs of various moments in the first case study: in the high panel, we see the beginning where all vehicles are uniformly spaced; in the center, we present the overall traffic at $t = 93$ s when high stop-and-go waves determine the whole dynamics; in the low panel, there is the situation at $t = 327$ s when traffic is almost completely stabilized.

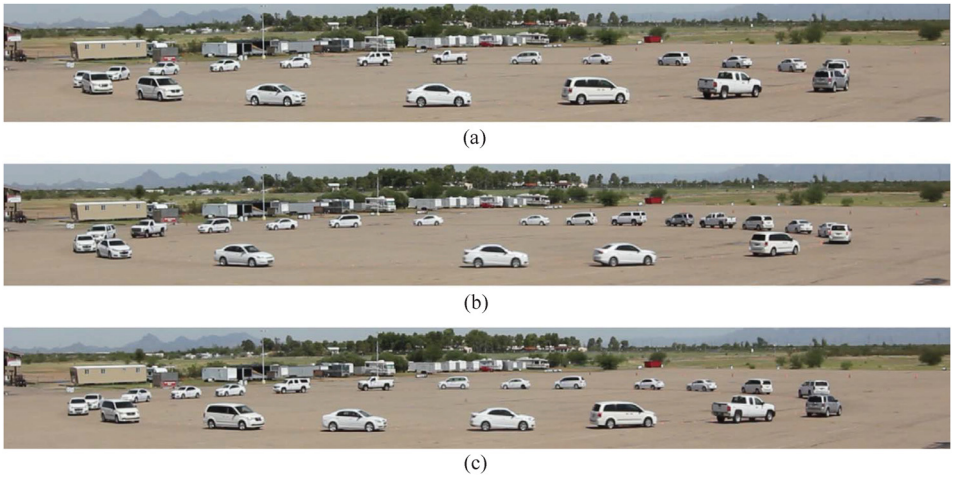

Figure 1: Real photographs: 21 vehicles on the ring road in various time instants. (a) Alignment of vehicles at start of the experiment, (b) alignment of vehicles 93 s into the experiment (presence of wave in back right), and (c) alignment of vehicles 327 s into the experiment (the AV is actively dampening the wave).

3.1 Control types

The presence of a unique AV inside the fleet proves experimentally that stop-and-go waves vanish or are dampened. The entity of such a phenomenon depends on the implemented control for the AV. As the primary aim is to stabilize traffic conditions to reach safety with a defined velocity [46], for each possible control strategy we have the following basic idea: from the evolution of traffic, a desired speed U is estimated and a commanded speed v^{cmd} is provided as input to a low-level controller that guides the AV. The different controllers of the AV are as follows: *Follower Stopper* (Experiment A), human-implemented control (Experiment B), *Proportional Integral (PI) with saturation* (Experiment C).

In Experiment A, following some instructions that are established by an external infrastructure, the AV tracks U in safety conditions and $v^{\mathrm{cmd}} < U$ when safety is needed. In Experiment B, the human pilot maintains an assigned speed and slows down only for possible collisions. In this case, the desired speed U, estimated through the length of the ring road and the time the AV needs for a complete pass, is communicated to the driver via radio. In Experiment C, the controller of the AV uses a PI logic to track v^{cmd} from information about the average speed of the vehicles in front. A saturation effect is also useful to ensure the safety distance.

3.2 Features of the experiments

In what follows, we give details about some features of the various experiments. In Experiment A, stop-and-go waves appear at 79 s and the control by the AV starts at 126 s. The commanded velocity, communicated to the driver by an external infrastructure, varies step by step from v^{cmd} = 6.50 m/s up to v^{cmd} = 8.00 m/s. The autonomy period and the experiment end are at 463 and 567 s, respectively.

For Experiment B, traffic waves occur at 55 s and the control, established by the human pilot of the AV, starts at 112 s with v^{cmd} = 6.25 m/s. The velocity has just a variation at 202 s. After the control is disabled at 300 s, the experiment ends at 409 s.

Experiment C has the first traffic wave at 161 s. The autonomy phase of the AV is activated at 218 s and v^{cmd} is adjusted by the automatic controller at each time instant until the end of the experiment (413 s).

Tables 1 and 2 report the main characteristics of the experiments, where we distinguish: an initial phase, IPH; an interval, TW, for traffic waves; intervals, indicated by C_i, where the control of the AV is activated; an interval DC, where the control is disabled and the experiment ends.

We provide information due to data analysis in Experiment A. For Experiments B and C, the obtained results are similar.

Table 3 presents an overview of the mean velocities for some vehicles along the ring track in Experiment A. Vehicle 21 is the AV, while 5 and 15 refer to vehicles that are within the fleet, approximately the same distance from the AV. From the results, obtained by not considering the outliers in the first and last intervals of the experiment, it follows that the mean velocities are not exactly the desired ones. The differences are due to the time required for all cars to adjust to the desired speed established by the AV. Note that, when stop-and-go

Table 1: Characteristics for Experiment A

Start	IPH = [0, 79[s
Waves	TW = [79, 126[s
Control	C_1 = [126, 222[s, v^{cmd} = 6.50 m/s
	C_2 = [222, 292[s, v^{cmd} = 7.00 m/s
	C_3 = [292, 347[s, v^{cmd} = 7.50 m/s
	C_4 = [347, 415[s, v^{cmd} = 8.00 m/s
	C_5 = [415, 463[s, v^{cmd} = 7.50 m/s
Disabled control	DC = [463,567] s

Table 2: Features for Experiments B and C

Experiment	B	C
Start	IPH = [0, 55[s	IPH = [0, 161[s
Waves	TW = [55, 112[s	TW = [161, 218[s
Control	C_1 = [112, 202[s, v^{cmd} = 6.25 m/s, C_2 = [202, 300[s, v^{cmd} = 7.15 m/s	C_1 = [218, 413] s
Disabled control	DC = [300, 409] s	—

Table 3: Mean velocities, expressed in m/s, for vehicles 5, 15, and 21 (AV) in the various time intervals (TIs) of Experiment A

TI	IPH	TW	C_1	C_2	C_3	C_4	C_5	DC
Vehicle 5	6.33	6.08	6.10	6.61	7.19	6.79	6.61	7.28
Vehicle 15	6.24	6.55	6.09	6.65	6.86	6.84	6.67	7.27
Vehicle 21 (AV)	6.13	6.34	5.94	6.58	7.12	6.78	6.69	7.34

waves arise, the mean velocities are, as expected, quite variable. During the control intervals, the regularization effect is more obvious. For instance, in C_2, C_4, and C_5 all vehicles have almost the same mean velocity. When the control is disabled in DC, a regularization phenomenon is still present and does not disappear immediately. This is confirmed by the almost similar values of the mean velocities.

Figure 2 shows the dynamics of velocities for the AV (black line) and vehicles 5 and 15 (blue and orange curves, respectively) in Experiment A. In the interval TW, velocities have high variations due to stop-and-go waves and the AV moves following an almost regular sinusoidal tune. For the other vehicles, the situation is similar but the amplitude of the oscillation is less marked for the car that is further away from the AV. The traffic is drastically dampened when the control is activated for the AV. In particular, in C_1 stop-and-go waves are reduced but this effect is not completely evident as the commanded velocity for the AV is 6.50 m/s, different from that of the overall traffic. In C_2, v^{cmd} becomes 7.00 m/s, a value comparable to the average speed of the entire fleet. This in turn creates more regularity in traffic dynamics, with a consequent reduction of possible variations in velocities.

For Experiments B and C, we obtain similar features that are not considered here.

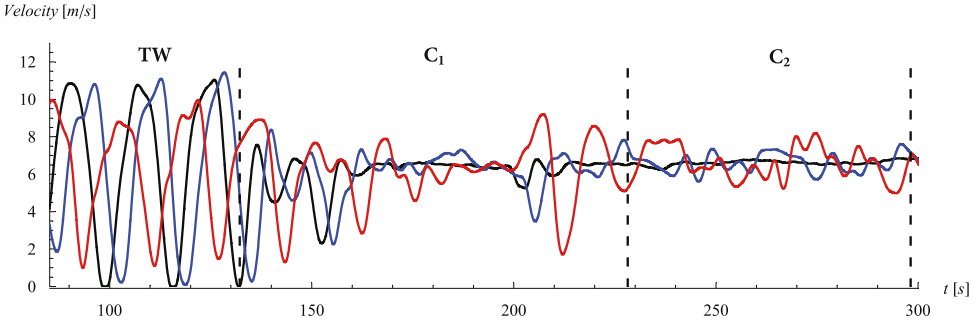

Figure 2: Velocities of the AV (black) and vehicles 5 (in blue) and 15 (in orange) in Experiment A: comparisons among velocities in TIs TW, C_1, and C_2.

4 Numerical results

This section shows some numerical results. First, we consider the results for PM emissions; then, we discuss the concentrations of pollutants at ground level and examine the effects due to the horizontal diffusion.

System (20) is solved using advanced approaches for time step sizes due to a high degree of stiffness. The numerical solution is found via the Matlab tool *ode23s* that combines an adaptive time step size and an implicit Runge-Kutta method. Note that, as source terms are defined on time scales larger than those of chemical reactions, possible intermediate time values are needed, and further interpolations are required. The equations for concentrations in the case of horizontal diffusion are numerically solved by finite differences. The advection term for the wind is treated by an up-winding approach in space and discretized explicitly in time. Finally, the source terms are pointwise explicitly approximated in time. If necessary, they are interpolated in case of various time scales. Details about numerical methods are in [31,33,47].

4.1 Estimation of PM emissions

Figures 3–5 show the evolution of PM emissions (indicated by E_{TOT}) vs time. The average emissions (AEs) in the critical intervals of type TW are as follows: 2.76 mg/s for Experiment A, 2.23 mg/s for Experiment B, and 1.81 mg/s for Experiment C. Indeed, Experiment A represents the worst case and all case studies show different features before the activation of possible control strategies.

In Experiment A, traffic waves are already dampened in C_1 but the highest reduction occurs in C_2 (best control interval, green check mark in Figure 3) when the AV and the other vehicles move all at a speed that is about the commanded one, $v^{\mathrm{cmd}} = 7.00$ m/s. When the control of the AV is disabled in the interval DC, traffic waves reappear and the AE becomes higher (albeit slightly) than that of the interval IPH. Table 4 shows the emission average values (expressed in milligrams/second [mg/s] and grams/minute [g/min]) for all TIs of Experiment A.

In Experiment B, when the pilot of the AV drives in C_1 at $v^{\mathrm{cmd}} = 6.25$ m/s, traffic waves become lower and, consequently, the AE decreases. When v^{cmd} becomes 7.15 m/s in C_2 (best control interval, green check mark in Figure 4), all vehicles have almost the same speed, i.e., the phenomenon is similar to that of Experiment A.

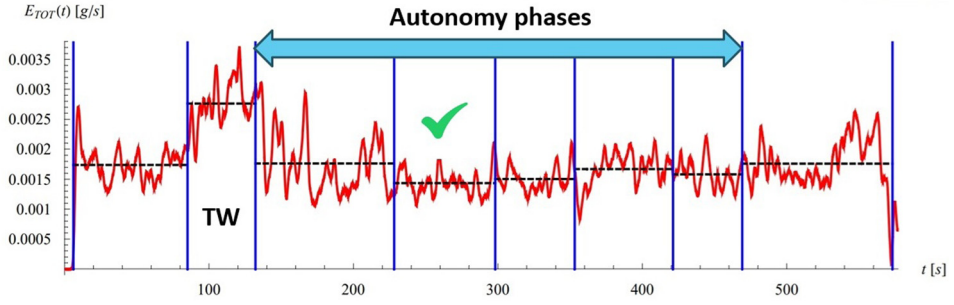

Figure 3: Red line: PM emissions for Experiment A. Dashed black lines: average values in the various TIs.

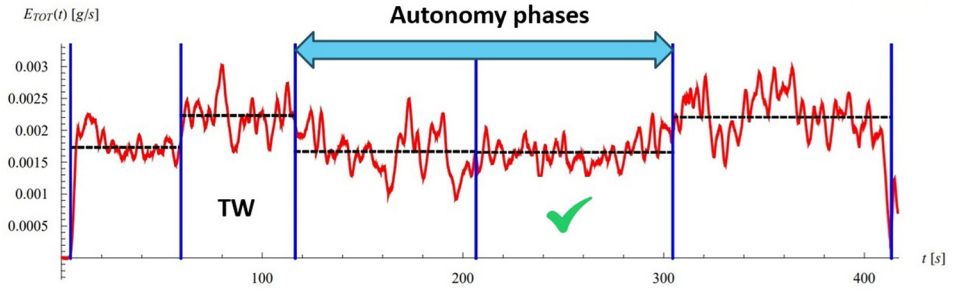

Figure 4: PM emissions for Experiment B (red line), and average values in TIs (dashed black lines).

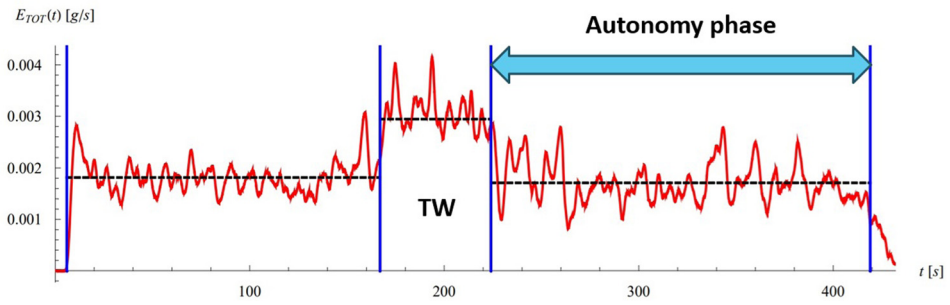

Figure 5: Red line: evolution of PM emissions for Experiment C. Dashed black lines: average values in different TIs.

Table 4: AEs for different TIs in Experiment A

TIs [s]	AEs [mg/s]	AEs [g/min]
IPH	1.74	0.104
TW	2.76	0.166
C_1	1.76	0.106
C_2	1.43	0.086
C_3	1.50	0.090
C_4	1.67	0.100
C_5	1.58	0.095
DC	1.76	0.106

Table 5: Experiment B: AEs for different TIs

TIs [s]	AEs [mg/s]	AEs [g/min]
IPH	1.73	0.104
TW	2.23	0.134
C_1	1.67	0.100
C_2	1.65	0.099
DC	2.20	0.132

Note that PM emissions are, indeed, almost similar in C_1 and C_2. When the control is disabled in DC, as expected the AE increases. The corresponding values are in Table 5 for Experiment B.

For Experiment C, when the control is activated in C_1, traffic waves are mitigated and the AE decreases. Note that the commanded velocity is highly variable due to the automatic logic implemented on the AV. This is also reflected in emissions that, although lower in the control interval, appear irregular in Figure 5. In Table 6, values of AEs are presented for Experiment C in all TIs.

For all experiments, PM emissions are dampened when control is activated on the unique AV of the fleet in consideration. The percentage reduction is different in the various experiments as a result of the used control strategy. Assume that R_i indicates the percentage reduction of particulate emissions for Experiment i, $i \in \{A, B, C\}$, i.e., R_i shows the decrease from the interval TW to the best control interval for Experiment i. We have

$$R_A = 48.04\%, \quad R_B = 25.38\%, \quad R_C = 41.98\%.$$

We note that Experiments A and C are almost similar in terms of decrease of PM emissions, unlike Experiment B for which reductions are about half those of Experiment A. This is predictable for Experiment B, for which only the human pilot determines the real control action.

Table 6: AEs for Experiment C in different TIs

TIs [s]	AEs [mg/s]	AEs [g/min]
IPH	1.81	0.109
TW	2.94	0.177
C_1	1.70	0.103

Now we provide information about the variations in PM emissions. In Figure 6, we consider the normalized derivative of $E_{\mathrm{TOT}}(t)$ in TW and in all control intervals for Experiment A. It is shown that the PM emissions have positive variations in TW and this confirms the increase of $E_{\mathrm{TOT}}(t)$. When the control strategy starts in C_1, the derivative becomes abruptly negative, which indicates the dampening of stop-and-go waves and the consequent decrease of $E_{\mathrm{TOT}}(t)$. In C_2, the overall traffic is more regular, hence creating a sinusoidal trend in oscillations. Although the mean values for PM emissions are slightly higher in C_3, C_4, and C_5 w.r.t. the phenomenon in C_2, the control of the AV is still active and this creates almost regular variations. Indeed, the peak in C_4 derives from the deviation of v^{cmd} from the average traffic speed. Hence, while there is still control, the damping of traffic waves is strongly due to the way the AV exerts control, and stop-and-go waves tend to reappear when the control logic obeys dynamics different from the average traffic. Finally, in C_5, v^{cmd} assumes the value observed in C_3, thus stabilizing the phenomenon.

Finally, in Figure 7 we present for Experiment A a comparison between NO_x and PM emissions, the former described in [48]. The percentage reduction for emissions of nitrogen oxides in the best control interval C_2 is 23.30%, about one half the corresponding decrease for PM, 50%. Indeed, the used model for the emissions estimation presents similar features for either NO_x or PM. In Figure 7, we show the emissions normalized variations for the two types of gases in TIs TW and C_i, $i = 1, \ldots, 5$. In the presence of stop-and-go waves, the two variations have a different evolution but the shapes are quite similar and almost coincident when the traffic becomes stable (at about 100 s). This means that particulate and nitrogen oxides have similar features, and possible phenomena due to other polluting agents are less evident. When the control of the AV is activated in C_1, the two variations are still similar until about 160 s but then become different. This is due to the effects of the AV whose control strategy modifies the traffic and, hence, the concentration of pollutants that compose PM. Indeed, at about 250 s (in C_2) the presence of the AV dampens more the traffic waves, and the variations of particulate and nitrogen oxides still become similar with low differences in their peak values. In C_3, PM and NO_x have almost coincident variations. In the remaining control intervals C_4 and C_5, we have similar situations.

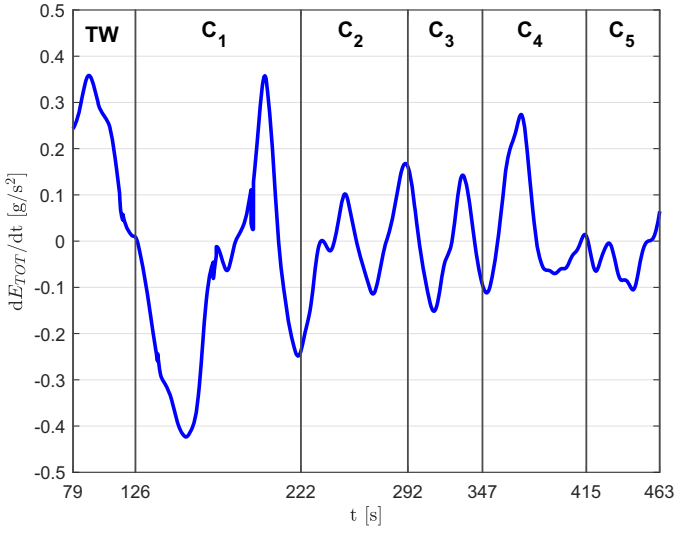

Figure 6: Normalized derivative of $E_{\mathrm{TOT}}(t)$, expressed in $\mathrm{g/s}^2$, in TIs TW, C_1, C_2, C_3, C_4, and C_5.

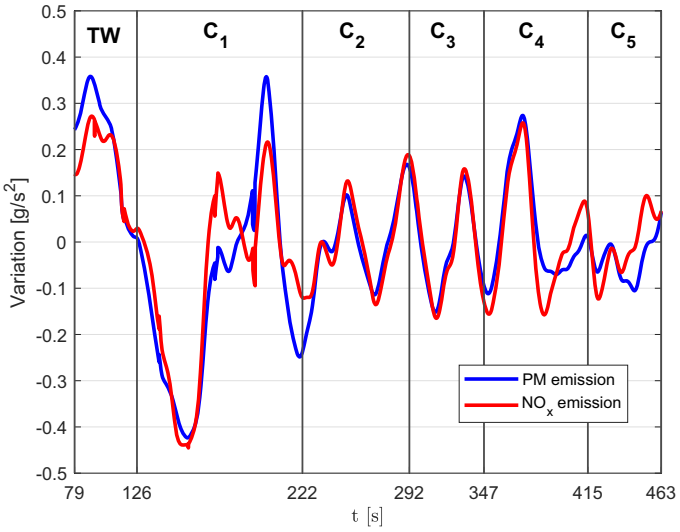

Figure 7: PM (blue) and NO_x (red) emissions normalized variations, expressed in g/s^2, in TIs TW and C_i, $i = 1,\dots, 5$.

From the obtained results, we obtain that the control of the AV stabilizes different types of emissions in the same way.

For Experiments B and C, the normalized derivatives for emissions present similar characteristics.

4.2 Pollutants at ground level

The concentrations of pollutants along the ring road at street level are estimated by finding solutions to system (24). In order to show the effects of concentration reduction due to the presence of AVs, we analyze separate cases: experiment phases when high traffic waves appear (AV with disabled control); TIs when autonomous driving dampens stop-and-go waves (AV with exerted control).

By using approaches that deal with stiff features of system (24), see [33], we find numerical solutions on a TI $I = [0, T]$ by a suitable choice of source terms (21). As we need simulations over a larger time horizon, the source term signal is prolonged by repeating the emission profile in I, namely: we obtain a periodic emission profile from the experimental data in a given phase (traffic waves or autonomy). We consider the following notations to distinguish among the traffic sources in different experiments and time intervals: $S^P_{\Gamma,\Phi}$ is the repetition, over I, of the source term in the TI $\Phi \in \{TW, C_i\}$ for pollutant $P \in \{NO_x, SO_x, PM\}$ in case of Experiment $\Gamma \in \{A, B, C\}$. For all simulations, we assume that: chemical species are estimated for each volume of size Δx^3, with $\Delta x = L\pi^{-1}$, where $L = 260$ m is the length of the ring track; $T = 30$ min; the concentrations at $t = 0$, indicated by $[\cdot]_0$, are as follows:

$$
\begin{aligned}
[O]_0 = [O_3]_0 &= 0, & [O_2]_0 &= 5.02\cdot 10^{18}\,\text{mol/cm}^3,\\
[NO]_0 &= (1-p)S^{NO_x}_{\Gamma,\Phi}(0), & [NO_2]_0 &= pS^{NO_x}_{\Gamma,\Phi}(0),\\
[SO]_0 &= 2.5\cdot 10^{18}\,\text{mol/km}^3, & [SO_2]_0 = [SO_3]_0 &= 4\cdot 10^{16}\,\text{mol/km}^3,\\
[PM_{10}]_0 &= S^{PM}_{\Gamma,\Phi}(0), & [PM_{2.5}]_0 &= \beta S^{PM}_{\Gamma,\Phi}(0),
\end{aligned}
$$

where $p = 0.15$. For the pollutants that compose PM_{10}, see equation (22), we consider $\alpha_1 = \alpha_2 = 0.5$. Note that, following the approach of [30], we obtain $S^{SO_x}_{\Gamma,\Phi}(0) = 0\ \forall t \in [0, T]$ and the evolution of SO_x is dependent on only the initial conditions.

In (24), using $S^{NO_x}_{A,TW}$ and $S^{PM}_{A,TW}$ that refer to stop-and-go waves in Experiment A, we obtain Figures 8–10 for some pollutants estimated until 90 min. In Figure 8, we have O_2 (left, dashed blue line) and O_3 (right, continuous black

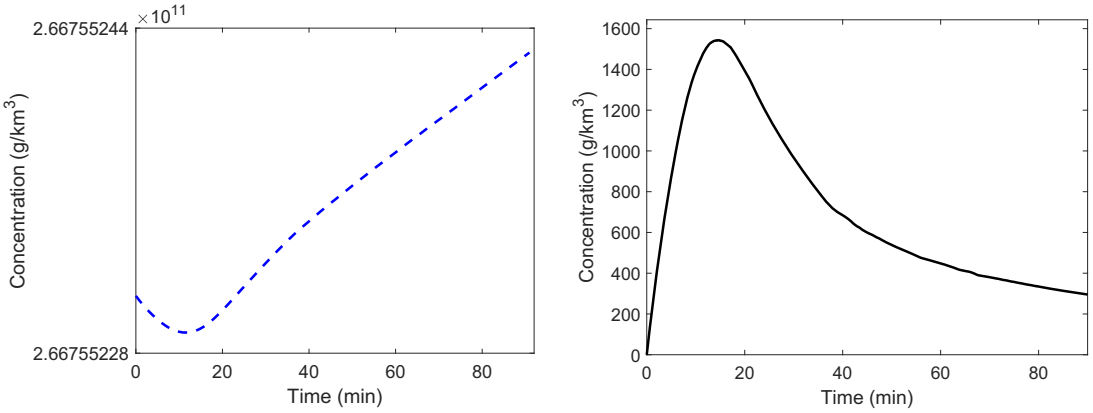

Figure 8: Concentrations (g/km^3) for O_2 (left, dashed blue line) and O_3 (right, continuous black line) vs time by solving (24) via $S_{A,\mathrm{TW}}^{\mathrm{NO_x}}$ and $S_{A,\mathrm{TW}}^{\mathrm{PM}}$.

line). Note that the graph of oxygen remains almost constant, unlike ozone which has first a fast growth, reaches a maximum, and then decreases. Precisely, when O_3 is maximum, O_2 has its minimum. The slow evolution of oxygen confirms its property as a vital gas while, as expected, ozone tends to increase due to the high stop-and-go

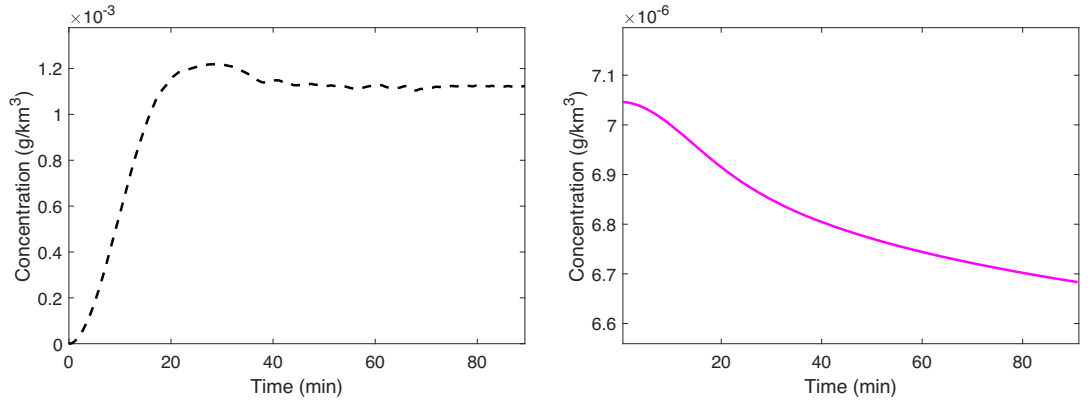

Figure 9: Concentrations (g/km^3) for O (left, dashed black line) and SO_2 (right, magenta line) vs time in case of solution of (24) by $S_{A,\mathrm{TW}}^{\mathrm{NO_x}}$ and $S_{A,\mathrm{TW}}^{\mathrm{PM}}$.

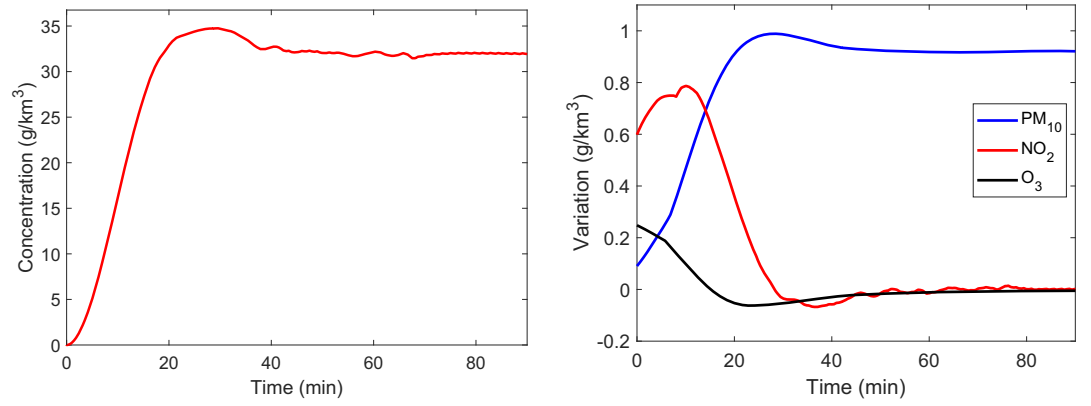

Figure 10: Left: Concentrations (g/km^3) for NO_2 (left, continuous red line) and normalized variation rates for PM_{10}, NO_2 and O_3 (right) by solving (24) via $S_{A,\mathrm{TW}}^{\mathrm{NO_x}}$ and $S_{A,\mathrm{TW}}^{\mathrm{PM}}$.

waves on the ring track. However, such pollutant agent decays naturally due to the deterioration reactions in system (24). In Figure 9, we see that O has a low concentration and quickly reaches a steady state, while SO_2 decreases due to the decay of O_3. Finally, Figure 10 presents NO_2 (left, continuous red line) and the normalized variations for PM_{10}, NO_2, and O_3 (right, see legend). Nitrogen oxides increase due to the highest traffic waves, but then it reaches a steady state. On the other hand, all variations of pollutants remain bounded but the highest values occur only for particulate.

The concentrations of pollutants O_3, NO_2, SO_2, and PM_{10} at T are as follows:

$$[O_3] = 0.9669 \text{ kg/km}^3, \qquad [NO_2] = 0.0347 \text{ kg/km}^3,$$
$$[SO_2] = 6.8119 \cdot 10^{-9} \text{ kg/km}^3, \qquad [PM_{10}] = 1940.3 \text{ kg/km}^3.$$

Figure 11 shows the percentage variations at T of $[O_3]$, $[NO_2]$, $[SO_2]$, and $[PM_{10}]$, obtained by source terms $S^{NO_x}_{A,C_i}$ and S^{PM}_{A,C_i}, $i = 1, \dots, 5$, and the variation percentages w.r.t. $S^{NO_x}_{A,TW}$ and $S^{PM}_{A,TW}$. In the control intervals for the AV, there is almost a whole decrease in the concentrations of pollutants. In particular, the best control period is C_2 for O_3, NO_2, and SO_2. Indeed, for the concentration of PM_{10}, C_3 is the interval with highest decrease. However, as C_2 and C_3 almost show the same variation for PM_{10}, we conclude that C_2 presents the best decrease for all the considered pollutants. Finally, from [28] the FC is 24.1l/100 km for the TW interval in Experiment A. It is shown that the highest variation occurs in C_3, where FC decreases of about 39.32%.

For Experiment B, computing the solutions of system (24) by the source terms $S^{NO_x}_{B,TW}$ and $S^{PM}_{B,TW}$, and $S^{NO_x}_{B,C_i}$ and S^{PM}_{B,C_i}, $i = 1, 2$, the behavior of concentrations is similar to Experiment A. For $S^{NO_x}_{B,TW}$ and $S^{PM}_{B,TW}$, the final values are as follows:

$$[O_3] = 0.7916 \text{ kg/km}^3, \qquad [NO_2] = 0.023 \text{ kg/km}^3,$$
$$[SO_2] = 5.5394 \text{ kg/km}^3, \qquad [PM_{10}] = 1580.1 \text{ kg/km}^3$$

and, in the TW phase for Experiment B, the FC is 21.8 l/100km. Decreases, variations of pollutants, and FC in control intervals are given in Table 7. There is a unique best control period (C_2) for which we obtain the highest decrease for pollutants O_3, NO_2, SO_2, and PM_{10}. FC has the most meaningful variation in C_2 as well.

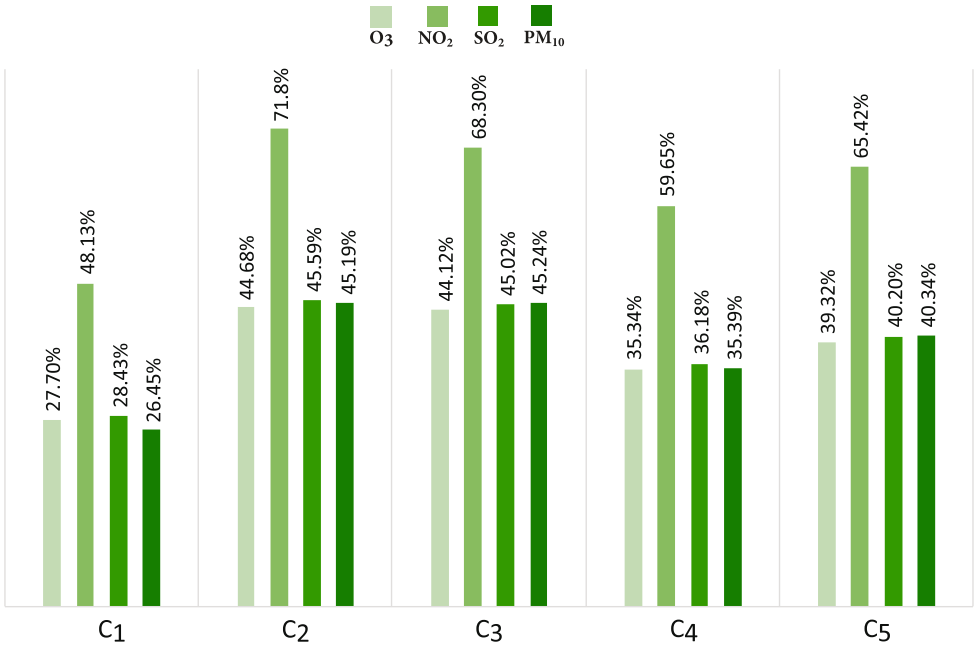

Figure 11: Percentage variations for the concentrations, at $T = 30$, of principal pollutants in cases of source terms for $S^{NO_x}_{A,C_i}$ and S^{PM}_{A,C_i}, $i = 1, \dots, 5$, compared to $S^{NO_x}_{A,TW}$ and $S^{PM}_{A,TW}$.

Table 7: Concentrations (C) of pollutants at $T = 30$ for $S^{NO_x}_{B,C_i}$ and S^{PM}_{B,C_i}, $i = 1, 2$, and variations (V) referred to $S^{NO_x}_{B,TW}$ and $S^{PM}_{B,TW}$; FC in C_i and variations (VF) referred to the TW interval of Experiment B

Source terms	C [kg/km^3]	V [%]	FC [l/100 km], VF [%]
$S^{NO_x}_{B,C_1}$, S^{PM}_{B,C_1}	$[O_3] = 0.6652$	–15.96	
	$[NO_2] = 0.0163$	–29.00	17.8, –18.35
	$[SO_2] = 4.6325$	–16.37	
	$[PM_{10}] = 1394.2$	–11.76	
$S^{NO_x}_{B,C_2}$, S^{PM}_{B,C_2}	$[O_3] = 0.6266$	–20.84	
	$[NO_2] = 0.0143$	–39.00	17.1, –21.56
	$[SO_2] = 4.3571$	–21.34	
	$[PM_{10}] = 1293.9$	–18.11	

Finally, we consider the solution to system (24) by $S^{NO_x}_{C,TW}$ and $S^{PM}_{C,TW}$, and $S^{NO_x}_{C,C_1}$ and S^{PM}_{C,C_1} (Experiment C). For $S^{NO_x}_{C,TW}$ and $S^{PM}_{C,TW}$, the final values of concentrations are as follows:

$$[O_3] = 0.8705 \text{ kg/km}^3, \quad [NO_2] = 0.028 \text{ kg/km}^3,$$
$$[SO_2] = 6.1103 \text{ kg/km}^3, \quad [PM_{10}] = 1872.9 \text{ kg/km}^3.$$

When the controller is activated in C_1, we obtain at the final time T:

$$[O_3] = 0.7391 \text{ kg/km}^3, \quad [NO_2] = 0.020 \text{ kg/km}^3,$$
$$[SO_2] = 5.1613 \text{ kg/km}^3, \quad [PM_{10}] = 1686.1 \text{ kg/km}^3.$$

Hence, during the autonomy phase, the concentrations of O_3, NO_2, SO_2, and PM_{10} decrease by about 15%, 29%, 16%, and 10%, respectively, while FC is reduced by about 21%.

Table 8 shows comparisons among the final values of concentration for the principal pollutants during intervals of type TW and in the best autonomy phases. The variations of pollutants are higher for Experiment A and decrease of about a half in Experiment B, with the unique exception of PM_{10}. For Experiment C, the lowest variations occur although, compared to Experiment B, they are almost comparable for pollutants O_3, NO_2, and SO_2. We conclude that the three different control strategies, used in the experiments, allow meaningful variations in the concentration of pollutants. Experiment A is the best in terms of decrease, hence AVs, if controlled by an external input decided by an infrastructure (control of type *Follower Stopper*), perform the better results in terms of traffic stabilization. When simple communications guide the human pilot in Experiment B (control of type *trained human driver*), decreases occur but the human component alone does not guarantee high reductions. For Experiment C which deals with control strategies based on local inform-

Table 8: Concentrations of the principal pollutants at $T = 30$ in TW (C_{TW}) and in the best control interval ($C_{C,best}$) for each experiment; variations (V) between the concentrations in the different TIs

Experiment	C_{TW} [kg/km^3]	$C_{AUT,best}$ [kg/km^3]	V [%]
A	$[O_3] = 0.9669$	$[O_3] = 0.5348$	–44.68
	$[NO_2] = 0.0347$	$[NO_2] = 0.010$	–71.18
	$[SO_2] = 6.8119$	$[SO_2] = 3.7059$	–45.59
	$[PM_{10}] = 1940.3$	$[PM_{10}] = 1063.3$	–45.19
B	$[O_3] = 0.7916$	$[O_3] = 0.6266$	–20.84
	$[NO_2] = 0.023$	$[NO_2] = 0.0143$	–39.00
	$[SO_2] = 5.5394$	$[SO_2] = 4.3571$	–21.34
	$[PM_{10}] = 1580.1$	$[PM_{10}] = 1293.9$	–18.11
C	$[O_3] = 0.8705$	$[O_3] = 0.07391$	–15.09
	$[NO_2] = 0.028$	$[NO_2] = 0.0201$	–28.57
	$[SO_2] = 6.1103$	$[SO_2] = 5.1613$	–15.53
	$[PM_{10}] = 1872.9$	$[PM_{10}] = 1686.1$	–9.97

ation (control design of type *PI controller with saturation*), we have similar features to Experiment B. Indeed, Experiment C shows quite different variations compared to other cases, hence indicating that the results are dependent on the experimental conditions.

Therefore, the control with infrastructure communication allows the best performances, while those with human actuator or local controller have lesser, but still significant, effects.

4.3 Horizontal diffusion of pollutants

Now we study the horizontal diffusion of pollutants. We simulate a scenario (Figure 12), that illustrates the two-dimensional vertical cross-section of the roadway, with a hole in the domain corresponding to a green barrier that acts as a sink for pollutants.

We consider the domain Ω described in Section 2.3, with L_x = 500 m and L_y = 0.5 m. A green wall of dimensions [250, 480] m × [0.1, 0.15] m and height 0.5 m is located in Ω. The domain is described by a numerical grid with dx = 5 m and dy = 0.02 m. The concentration of pollutants per unit of volume is defined by

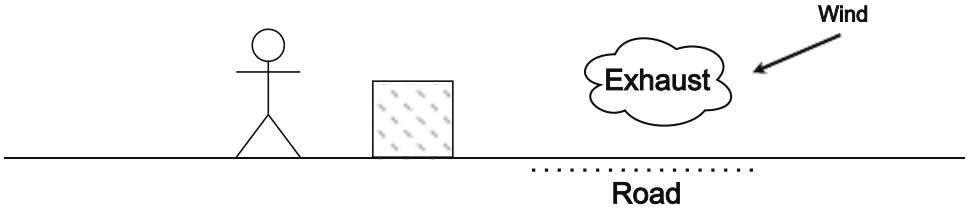

Figure 12: Scenario with a point-source introduction of pollutants and a green barrier implemented as a hole (greyed region).

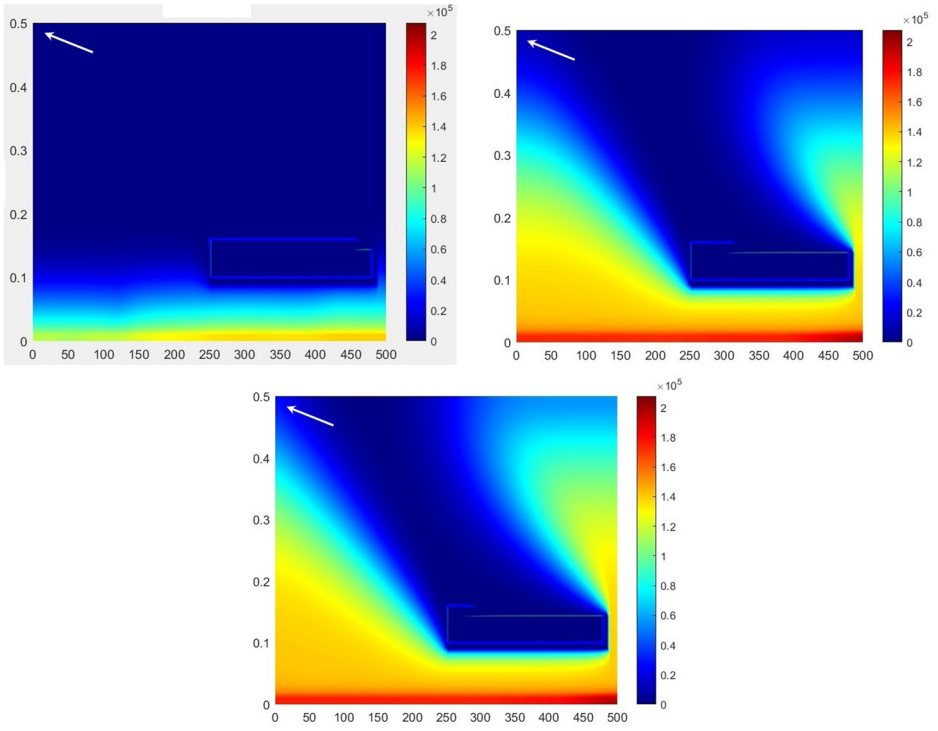

Figure 13: Horizontal diffusion of ozone concentration (g/km^3) in Ω in different time instants t. Up left: t = 3. Up right: t = 15. Down: t = 30. White arrow: direction of the wind.

setting: $\mathbf{\Gamma}$ constant along the third component dz, equal to dy; zero initial conditions, except oxygen that is assumed constant, see the previous subsection; $\mu = 10^{-8}$ km^2/h for all pollutants; total simulation TI $[0, T]$ with $T = 30$ min. Finally, we consider: a wind vector $\mathbf{w}$ that is

$$\mathbf{w} = (-0.8\,\text{km/h})\mathbf{i} + (0.001\,\text{km/h})\mathbf{j},$$

where $\mathbf{i}$ and $\mathbf{j}$ are the unit vectors of the horizontal and vertical axes, respectively. The road is represented by the lower side of Ω, where the sources of emissions act.

Assuming source emissions due to $S^{\text{NO}_x}_{A,\text{TW}}$ and $S^{\text{PM}}_{A,\text{TW}}$, we have results for O_3 in Figure 13 and PM_{10} in Figure 14, in the case of Experiment A.

From Figure 13, we obtain that, already in the initial moments of observation, O_3 grows rapidly at approximately $y = 0$. In subsequent moments, O_3 spreads along the domain Ω, but the green barrier is an obstacle for a complete diffusion (see $t = 15$). At the final instant $t = 30$, O_3 has increased in $[400, 500]$ m × $[0.3, 0.4]$ m but the overall diffusion along Ω remains quite discontinuous. The average value of O_3 at $t = 30$ is about 0.2 kg/km^3 for people walking near the green barrier, i.e., at about $[250, 480]$ m × $[0.15, 0.2]$ m in Ω. Finally, we conclude that the barrier is very effective for ozone protection, especially in the upper edge of the domain ($y \simeq 0.5$ m).

As for PM_{10}, Figure 14 (up left) shows that, at $t = 3$, particulate levels are very low, except the subdomains $[0, 100]$ m × $[0.11, 0.3]$ m and $[400, 500]$ m × $[0.11, 0.3]$ m. When $t = 15$, the green barrier prevents a complete diffusion of the pollutant that increases at the edges of Ω. Finally, at $t = 30$, PM_{10} reaches its highest value, about 30 kg/km^3, in $[400, 500]$ m × $[0.3, 0.45]$ m. Indeed, the particulate values are quite different from those related to O_3: people near the upper edge of the domain are not fully protected by the diffusion, as confirmed by the discontinuous pollutant levels. This indicates that green barriers are not very efficient for protection against particulate pollution.

For Experiments B and C, we obtain similar results that are omitted here.

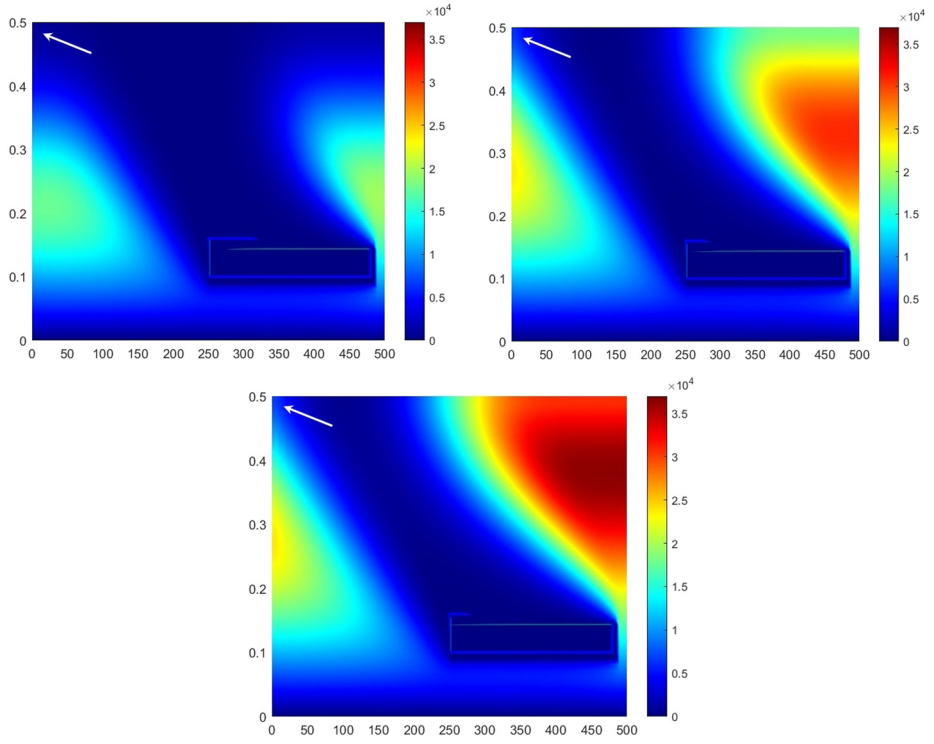

Figure 14: Horizontal diffusion for PM_{10} concentration (g/km^3) in Ω in various time instants t. Up left: $t = 3$. Up right: $t = 15$. Down: $t = 30$. White arrow: direction of the wind.

5 Conclusions

The results of this article show how PM emissions are influenced by traffic conditions and how their diffusion at ground level is affected by green barriers. First, the used approach proved that the presence of a unique AV in a fleet leads to several benefits: mitigation of stop-and-go waves, stabilization of vehicle flows, and reduction of PM emissions with a consequent decrease in concentration at ground level. Such phenomena were studied by three different controls implemented on the AV: infrastructure communication, human component, and local information. The first controller allowed better performances, but meaningful impacts were also obtained in the remaining cases.

The analysis of the horizontal diffusion in the presence of green barriers in urban contexts has found interesting features for different pollutant agents. In particular, green barriers have a very good screening effect for the diffusion of ozone. However, they do not reduce efficiently the effects of PM, with consequent risks to humans' health.

Future research activities aim to consider more complex traffic scenarios to estimate the PM emission and to provide more advanced tools to estimate the effect of diffusion as a function of different green barriers, such as bushes, trees, and green walls.

Funding information: The authors state that there is no funding.

Author contributions: All authors contributed equally to the manuscript and read and approved the final manuscript.

Conflict of interest: The authors state no conflict of interest.

References

[1] Y. Fan, Q. Meng, C. Weisel, S. Shalat, R. Laumback, P. Ohman-Strickland, et al., *Acute short-term exposures to* $PM_{2.5}$ *generated by vehicular emissions and cardiopulmonary effects in older adults*, Epidemiology **17** (2006), no. 6, S213–S214, DOI: http://dx.doi.org/10.1097/00001648-200611001-00544.

[2] M. Masiol, A. Hofer, S. Squizzato, R. Piazza, G. Rampazzo, and B. Pavoni, *Carcinogenic and mutagenic risk associated to airborne particle-phase polycyclic aromatic hydrocarbons: a source apportionment*, Atmos. Environ. **60** (2012), 375–382, DOI: https://doi.org/10.1016/j.atmosenv.2012.06.073.

[3] J. Rissler, E. Swietlicki, A. Bengtsson, C. Boman, J. Pagels, T. Sandstrom, et al., *Experimental determination of deposition of diesel exhaust particles in the human respiratory tract*, J. Aerosol Sci. **48** (2012), 18–33, DOI: https://doi.org/10.1016/j.jaerosci.2012.01.005.

[4] H. Fan, C. Zhao, and Y. Yang, *A comprehensive analysis of the spatio-temporal variation of urban air pollution in China during 2014-2018*, Atmos. Environ. **220** (2020), 117066, DOI: https://doi.org/10.1016/j.atmosenv.2019.117066.

[5] J. Rissler, E. Swietlicki, A. Bengtsson, C. Boman, J. Pagels, T. Sandstrom, et al., *Estimating the contribution of local primary emissions to particulate pollution using high-density station observations*, J. Geophys. Res. Atmos. **124** (2019), no. 3, 1648–1661, DOI: https://doi.org/10.1029/2018JD028888.

[6] S. Chen, J. Huang, L. Kang, H. Wang, X. Ma, Y. He, et al., *Emission, transport, and radiative effects of mineral dust from the Taklimakan and Gobi deserts: Comparison of measurements and model results*, Atmos. Chem. Phys. **17** (2017), no. 3, 2401–2421, DOI: https://doi.org/10.5194/acp-17-2401-2017.

[7] P. Tian, L. Zhang, J. Ma, K. Tang, L. Xu, Y. Wang, et al., *Radiative absorption enhancement of dust mixed with anthropogenic pollution over East Asia*, Atmos. Chem. Phys. **18** (2018), no. 11, 7815–7825, DOI: https://doi.org/10.5194/acp-18-7815-2018.

[8] U. A. Hvidtfeldt, M. Sørensen, C. Geels, M. Ketzel, J. Khan, A. Tjønneland, et al., *Long-term residential exposure to* $PM_{2.5}$, PM_{10}, *black carbon,* NO_2, *and ozone and mortality in a Danish cohort*, Environ. Int. **123** (2019), 265–272, DOI: https://doi.org/10.1016/j.envint.2018.12.010.

[9] A. Talbi, Y. Kerchich, R. Kerbachi, and M. Boughedaoui, *Assessment of annual air pollution levels with* PM_1, $PM_{2.5}$, PM_{10} *and associated heavy metals in Algiers, Algeria*, Environ. Pollut. **232** (2017), 252–263, DOI: https://doi.org/10.1016/j.envpol.2017.09.041.

[10] M. Mathissen, V. Scheer, R. Vogt, and T. Benter, *Investigation on the potential generation of ultrafine particles from the tire-road interface*, Atmos. Environ. **45** (2011), no. 34, 6172–6179, DOI: https://doi.org/10.1016/j.atmosenv.2011.08.032.

[11] A. Thorpe and R. M. Harrison, *Sources and properties of non-exhaust particulate matter from road traffic: a review*, Sci. Total Environ. **400** (2008), no. 1–3, 270–282, DOI: https://doi.org/10.1016/j.scitotenv.2008.06.007.
[12] H. Denier van der Gon, M. E. Gerlofs-Nijland, R. Gehrig, M. Gustafsson, N. Janssen, R. M. Harrison, et al., *The policy relevance of wear emissions from road transport, now and in the future – an international workshop report and consensus statement*, J. Air Waste Manage. **63** (2013), no. 2, 136–149, DOI: https://doi.org/10.1080/10962247.2012.741055.
[13] Y. Sugiyama, M. Fukui, M. Kikuchi, K. Hasebe, A. Nakayama, K. Nishinari, et al., *Traffic jams without bottlenecks-experimental evidence for the physical mechanism of the formation of a jam*, New J. Phys. **10** (2008), no. 3, 033001, DOI: https://doi.org/10.1088/1367-2630/10/3/033001.
[14] S.-i. Tadaki, M. Kikuchi, M. Fukui, A. Nakayama, K. Nishinari, A. Shibata, et al., *Phase transition in traffic jam experiment on a circuit*, New J. Phys. **15** (2013), no. 10, 103034, DOI: https://doi.org/10.1088/1367-2630/15/10/103034.
[15] F. Wu, R. E. Stern, S. Cui, M. L. Delle Monache, R. Bhadani, M. Bunting, et al., *Tracking vehicle trajectories and fuel rates in phantom traffic jams: Methodology and data*, Transport. Res. C: Emerging Technol. **99** (2019), 82–109, DOI: https://doi.org/10.1016/j.trc.2018.12.012.
[16] J. Liu, K. Kockelman, and A. Nichols, *Anticipating the emissions impacts of autonomous vehicles using the moves model*, Proceedings of the 95th Transportation Research Board Annual Meeting, Washington, DC.
[17] O. Servin, K. Boriboonsomsin, and M. Barth, *An energy and emissions impact evaluation of intelligent speed adaptation*, Proceedings of the IEEE Intelligent Transportation Systems Conference (ITSC), IEEE, 2006, pp. 1257–1262.
[18] K. Boriboonsomsin, M. J. Barth, W. Zhu, and A. Vu, *Eco-routing navigation system based on multisource historical and real-time traffic information*, IEEE Trans. Intell. Transport. Syst. **13** (2012), no. 4, 1694–1704, DOI: https://doi.org/10.1109/TITS.2012.2204051.
[19] F. Schäfer and R. Van Basshuysen, *Reduced Emissions and Fuel Consumption in Automobile Engines*, Springer Science & Business Media, Berlin, 2013.
[20] G. Fontaras, P. Pistikopoulos, and Z. Samaras, *Experimental evaluation of hybrid vehicle fuel economy and pollutant emissions over real-world simulation driving cycles*, Atmos. Environ. **42** (2008), no. 18, 4023–4035, DOI: https://doi.org/10.1016/j.atmosenv.2008.01.053.
[21] L. Chapman, *Transport and climate change: a review*, J. Transp. Geogr. **15** (2007), no. 5, 354–367, DOI: https://doi.org/10.1016/j.jtrangeo.2006.11.008.
[22] M. Barth and K. Boriboonsomsin, *Real-world carbon dioxide impacts of traffic congestion*, Transport. Res. Rec. Board **2058** (2008), no. 163–171, DOI: https://doi.org/10.3141/2058-20.
[23] F. An, M. Barth, J. Norbeck, and M. Ross, *Development of comprehensive modal emissions model: operating under hot-stabilized conditions*, Transport. Res. Record: Board **1587** (1997), 52–62, DOI: https://doi.org/10.3141/1587-07.
[24] D. Schuetzle, *Sampling of vehicle emissions for chemical analysis and biological testing*, Environ. Health Perspect. **47** (1983), 65, DOI: https://doi.org/10.1289/ehp.834765.
[25] M. André, M. Keller, A. Sjödin, M. Gadrat, I. Mc Crae, and P. Dilara, *The ARTEMIS European tools for estimating the transport pollutant emissions*, Proceedings of the 18th International Emission Inventories Conference, 2009, pp. 1–10.
[26] A. Cappiello, I. Chabini, E. K. Nam, A. Lue, and M. A. Zeid, *A statistical model of vehicle emissions and fuel consumption*, Proceedings of the 5th IEEE International Conference on Intelligent Transportation Systems (ITSC), IEEE, 2002, pp. 801–809.
[27] H. Teng, L. Yu, and Y. Qi, *Statistical microscale emission models incorporating acceleration and deceleration*, Proceedings of the 81st Transportation Research Board Annual Meeting, 2010, p. 29.
[28] R. E. Stern, S. Cui, M. L. Delle Monache, R. Bhadani, M. Bunting, M. Churchill, et al., *Dissipation of stop-and-go waves via control of autonomous vehicles: field experiments*, Transport. Res. C Emerging Technol. **89** (2018), 205–221, DOI: https://doi.org/10.1016/j.trc.2018.02.005.
[29] R. E. Stern, Y. Chen, M. Churchill, F. Wu, M. L. Delle Monache, B. Piccoli, et al., *Quantifying air quality benefits resulting from few autonomous vehicles stabilizing traffic*, Transp. Res. D Trans. Environ. **67** (2019), 351–365, DOI: https://doi.org/10.1016/j.trd.2018.12.008.
[30] L. I. Panis, S. Broekx, and R. Liu, *Modelling instantaneous traffic emission and the influence of traffic speed limits*, Sci. Total Environ. **371** (2006), 270–285, DOI: https://doi.org/10.1016/j.scitotenv.2006.08.017.
[31] C. Balzotti and M. Briani, *Estimate of traffic emissions through multiscale second order models with heterogeneous data*, Netw. Heterog. Media **17** (2022), no. 6, 863–892, DOI: https://doi.org/10.3934/nhm.2022030.
[32] C. Balzotti, M. Briani, B. De Filippo, and B. Piccoli, *Towards a comprehensive model for the impact of traffic patterns on air pollution*, Proceedings of the 6th International Conference on Vehicle Technology and Intelligent Transport Systems (VEHITS2020), vol. 1, 2020, pp. 221–228.
[33] C. Balzotti, M. Briani, B. De Filippo, and B. Piccoli, *A computational modular approach to evaluate* NO_x *emissions and ozone production due to vehicular traffic*, Discrete Contin. Dyn. Syst. Ser. B **27** (2022), no. 6, 3455–3486, DOI: https://doi.org/10.3934/dcdsb.2021192.
[34] J. H. Seinfeld and S. N. Pandis, *Atmospheric Chemistry and Physics: From Air Pollution to Climate Change*, John Wiley & Sons, New York, 2016.
[35] R. P. Wayne, *Chemistry of Atmospheres*, Clarendon Press, Oxford, 1991.
[36] D. J. Jacob, *Heterogeneous chemistry and tropospheric ozone*, Atmos. Environ. **34** (2000), no. 12, 2131–2159, DOI: https://doi.org/10.1016/S1352-2310(99)00462-8.
[37] F. Song, J. Y. Shin, R. Jusino-Atresino, and Y. Gao, *Relationships among the springtime ground-level NOx, O3 and NO3 in the vicinity of highways in the US East Coast*, Atmos. Pollut. Res. **2** (2011), no. 3, 374–383, DOI: https://doi.org/10.5094/APR.2011.042.

[38] R. Smit, L. Ntziachristos, and P. Boulter, *Validation of road vehicle and traffic emission models – A review and meta-analysis*, Atmos. Environ. **44** (2010), 2943–2953, DOI: https://doi.org/10.1016/j.atmosenv.2010.05.022.
[39] M. Z. Jacobson, *Fundamentals of Atmospheric Modeling*, Cambridge University Press, Cambridge, 2005.
[40] S. Manahan, *Environmental Chemistry*, CRC Press, Boca Raton, 2017.
[41] H. Omidvarborna, A. Kumar, and D.-S. Kim, NO_x *emissions from low-temperature combustion of biodiesel made of various feedstocks and blends*, Process. Technol. **140** (2015), 113–118, DOI: https://doi.org/10.1016/j.fuproc.2015.08.031.
[42] H. Fan, C. Zhao, Y. Yang, and X. Yang, *Spatio-temporal variations of the* $\mathrm{PM}_{2.5}/\mathrm{PM}_{10}$ *ratios and its application to air pollution type classification in China*, Front. Environ. Sci. **9**, Article 692440 (2021), 1–13, DOI: https://doi.org/10.3389/fenvs.2021.692440.
[43] D. C. Carslaw, S. D. Beevers, J. E. Tate, E. J. Westmoreland, and M. L. Williams, *Recent evidence concerning higher* NO_x *emissions from passenger cars and light duty vehicles*, Atmos. Environ. **45** (2011), 7053–7063, DOI: https://doi.org/10.1016/j.atmosenv.2011.09.063.
[44] B. Sportisse, *Fundamentals in Air Pollution: From Processes to Modelling*, Springer Science+Business Media, New York, 2010.
[45] K. V. Abhijith, P. Kumar, J. Gallagher, A. McNabola, R. Baldauf, F. Pilla, et al., *Air pollution abatement performances of green infrastructure in open road and built-up street canyon environments - A review*, Atmos. Environ. **162** (2017), 71–86, DOI: https://doi.org/10.1016/j.atmosenv.2017.05.014.
[46] S. Cui, B. Seibold, R. E. Stern, and D. B. Work, *Stabilizing traffic flow via a single autonomous vehicle: Possibilities and limitations*, 2017 IEEE Intelligent Vehicle Symposium (IV), IEEE, 2017, pp. 1336–1341.
[47] E. Hairer and G. Wanner, *Solving Ordinary Differential Equations II. Stiff and Differential-Algebraic Problem*, Second edition, Springer Series in Computational Mathematics, Springer-Verlag, Berlin, Heidelberg, New York, 1996.
[48] M. Briani, R. Manzo, B. Piccoli, and L. Rarità, *Estimation of* NO_x *and* O_3 *reduction by dissipating traffic waves*, Netw. Heterog. Media **19** (2024), no. 2, 822–841, DOI: https://doi.org/10.3934/nhm.2024037.